Acta Crystallographica Section D
Biological Crystallography
ISSN 0907-4449

Comparison of two T-state structures of regulatory-chain mutants of *Escherichia coli* aspartate transcarbamoylase suggests that His20 and Asp19 modulate the response to heterotropic effectors

Boguslaw Stec,[a]* Mark K. Williams,[b] Kimberly A. Stieglitz[b] and Evan R. Kantrowitz[b]

[a]Burnham Institute for Medical Research, La Jolla, CA 92037, USA, and [b]Department of Chemistry, Merkert Chemistry Center, Boston College, Chestnut Hill, MA 02467, USA

Correspondence e-mail: bstec@burnham.org

Received 22 June 2007
Accepted 24 October 2007

PDB References: ATCase, D19A mutant, 2qg9; H20A mutant, 2qgf, r2qgfsf.

Asp19 and His20 of *Escherichia coli* aspartate transcarbamoylase (EC 2.1.3.2) function in the binding of the triphosphate and ribose moieties of ATP and CTP and thereby may mediate important heterotropic regulation. The roles of these residues were investigated by individually mutating each of them to alanine and determining both the kinetic parameters and the structures of the mutant enzymes. The structures were determined by X-ray crystallography at 2.15 and 2.75 Å resolution for His20Ar and Asp19Ar, respectively. Analysis was carried out on the unliganded T-state form. The structures of the mutants did not show gross structural divergence from the canonical T-state, but showed small and systematic differences that were analyzed by global conformational analysis. Structural analysis and comparison with other regulatory-chain mutants confirmed that the Asp19Ar mutant represents the stabilized T-state, while structural analysis of the His20Ar form indicated that it represents an equilibrium shifted towards the R-state. Global analysis of the Asp19Ar and His20Ar enzymes suggested a possible role as molecular modulators of the heterotropic effects caused by the binding of nucleotides at the regulatory site. These studies highlighted the structural determinants of T- or R-state stabilization. Additionally, application of the 'consensus modeling' methodology combined with high-resolution data allowed the determination of unclear structural features contributing to nucleotide specificity and the role of the N-termini of the regulatory chains.

1. Introduction

For more than 40 years, aspartate transcarbamoylase (ATCase; EC 2.1.3.2) has served as a paradigm of allosteric regulation. Since the observation of Yates & Pardee (1956) that *Escherichia coli* aspartate transcarbamoylase is subject to feedback inhibition by cytidine and cytidine monophosphate and activation by adenosine triphosphate (Gerhart & Pardee, 1962), there has been an intense effort to understand its regulation. In addition to heterotropic control by nucleotides, the enzyme exhibits positive homotropic cooperativity between catalytic sites, shown experimentally by the sigmoidal dependence of its activity on the concentration of one of the substrates, aspartate (England & Hervé, 1994; Gerhart & Schachman, 1968).

ATCase catalyzes the first reaction in the pyrimidine-biosynthetic pathway: the condensation of carbamyl phosphate with aspartate to form phosphate and *N*-carbamyl L-aspartate, the precursor of the pyrimidine ring (Jones *et al.*, 1955; Reichard & Hanshoff, 1956). The reaction is ordered with the carbamyl phosphate binding first and creating

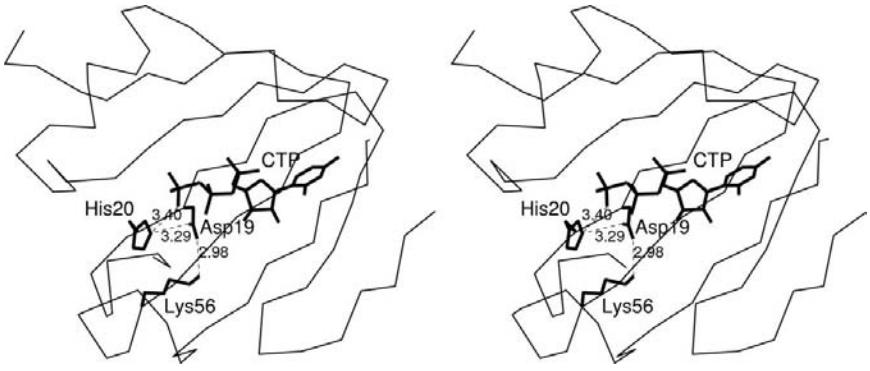

Figure 1
The hydrogen bonds to the CTP γ-phosphate made by the side chains of Asp19 and His20 as described by Kosman *et al.* (1993) (PDB code 1rah). A hydrogen-bonded network of residues is present in which Asp19 stabilizes the positive charge on the histidine.

conditions for aspartate binding. The enzyme only exhibits cooperativity upon aspartate binding. The enzyme can be activated or inhibited by nucleotides binding at a site located ~60 Å away on the regulatory subunit.

The way in which the holoenzyme regulatory and catalytic chains interact in the absence and presence of homotropic and heterotropic effectors, which initiate local structural changes such as altered interface contacts and subunit interactions before global changes shift the state of equilibrium of the enzyme, is under intense study. The enzyme is a dodecamer of 310 kDa comprised of six regulatory chains (17 kDa each), which assemble to form three regulatory dimers, and six catalytic chains (34 kDa each), which assemble to form two catalytic trimers[1]. The catalytic trimers are positioned face to face around a threefold axis and are joined by the three regulatory dimers. The X-ray structure revealed that both the catalytic and regulatory chains are composed of two separate folding domains. The aspartate and carbamoyl phosphate domains of the catalytic chain, previously named the polar and equatorial domains, are responsible for binding aspartate and carbamoyl phosphate substrates, respectively, while the allosteric and zinc domains of the regulatory chain are responsible for binding the regulatory nucleotides and a structural zinc, respectively.

X-ray structural work combined with kinetic studies indicated that the enzyme can assume two distinct structural and functional states: a low-activity T-state with a low affinity for substrate and a high-activity, high-affinity R-state. The resting enzyme is in a collapsed T-state, which upon binding substrates or substrate analogs such as *N*-phosphonacetyl L-aspartate (PALA) undergoes alteration of the quaternary structure to the relaxed R-state. These two states have been detected by sedimentation velocity (Howlett & Schachman, 1977), low-angle X-ray scattering studies (Hervé *et al.*, 1985; Moody *et al.*, 1979) and single-crystal X-ray crystallography (Ke *et al.*, 1988). This quaternary conformational change involves elongation of the molecule by 11 Å along the threefold axis coupled with rotation around this axis of catalytic trimers and the simultaneous rotation of the regulatory dimers around twofold axes that are perpendicular to the main axis (Ke *et al.*, 1988; Kosman *et al.*, 1993).

Numerous kinetic studies have elucidated the heterotropic effects in the enzyme. Alanine replacement of residues Thr2r–Leu7r[2] has been undertaken in order to analyze the role of the regulatory N-terminus in the heterotropic response (Dembowski & Kantrowitz, 1994). Lys6r was defined as being important for UTP inhibition of the enzyme in the absence and presence of CTP by salt-bridge formation with Glu62r. Further studies deleting the first ten residues of the regulatory chain showed marked effects on the kinetics of the heterotropic response, with a lower maximal velocity and a slight decrease in aspartate affinity (Sakash & Kantrowitz, 1998). More specifically, mutating Ile12r, which stabilizes nucleotides by direct backbone interaction (Stevens *et al.*, 1990), to alanine neither reduced nor eliminated the heterotropic response. Mutation of Glu62r to alanine eliminated the ability of the enzyme to discriminate between CTP and ATP, most likely because Glu62r indirectly participates in the binding of CTP (Sakash *et al.*, 2000).

Many structural studies also have addressed the role of the allosteric domain in heterotropic regulation. For example, both ATP- and CTP-liganded T-state structures of the wild-type enzyme and of some mutants (Honzatko *et al.*, 1982; Stevens *et al.*, 1990; Stieglitz *et al.*, 2004) have been obtained and their interactions with effectors have been described. The effector interactions included those occurring at amino acids Asp19 and His20 addressed here, which are within hydrogen-bonding distance of the CTP γ-phosphate (PDB code 1rah; Kosman *et al.*, 1993; Fig. 1).

In this study, His20Ar and Asp19Ar mutant enzymes[3] were constructed in order to determine how the two residues regulate the ability of the enzyme to discriminate between regulatory nucleotides. Kinetic analyses of the two mutants showed a loss of cooperativity and activity. Furthermore, CTP and ATP were not as effective in their respective abilities to inhibit and activate the mutant enzymes compared with the wild-type enzyme (Williams & Kantrowitz, 1998), suggesting overall that His20Ar or Asp19Ar substitutions alter the enzyme conformation to one in which the R- or T-state is

[1] Regulatory chains r1 and r6 comprise one regulatory dimer. r2–r5 and r3–r6 comprise the other regulatory subunits. Catalytic chains c1, c2 and c3 comprise the upper catalytic subunit, while chains c4, c5 and c6 comprise the lower catalytic subunit. Chain c4 is below c1, while c5 and c6 are below chains c2 and c3, respectively.

[2] A 'c' or 'r' appended to a residue number indicates that the residue is in the catalytic or regulatory chain of aspartate transcarbamoylase, respectively. When necessary, a number is appended to the chain to designate the particular regulatory or catalytic chain.

[3] Mutant enzymes are designated by the three-letter code of the wild-type amino acid, followed by the residue number, followed by the one-letter code of the substitution. For example, histidine 20 of the regulatory (r) chain mutated to alanine is designated His20Ar.

Table 1
Data-collection and refinement statistics for T-state structures of the Asp19Ar and His20Ar enzymes.

	Asp19Ar	His20Ar
Space group	*P*321	*P*321
Unit-cell parameters (Å)	$a = b = 122.2$, $c = 142.4$	$a = b = 122.3$, $c = 142.5$
$R_{\rm merge}$	0.101	0.099
Resolution range of refinement (Å)	10.0–2.8	10.0–2.2
No. of reflections	28103	59318
Completeness (%)	91.3	94.8
Redundancy	2.6	3.3
Final R factor/$R_{\rm free}$	0.191/0.244	0.197/0.223
R.m.s. deviations		
Bond lengths (Å)	0.017	0.015
Bond angles	2.2	1.8
Dihedral angles	25.6	25.7
Improper angles	2.0	1.6
Temperature factors (Å^2)		
Overall	27.3	33.1
c1	23.7	28.9
r1	38.3	48.9
c6	20.0	22.1
r6	32.6	47. 6

stabilized, respectively. To investigate the structural determinants of these mutations, which are potentially associated with altered equilibrium and kinetic properties, the mutants were crystallized in the unliganded T-state and structures were determined at 2.15 and 2.75 Å for His20Ar and Asp19Ar, respectively. Structural analysis of the Asp19 and His20 interactions correlates well with previous functional studies concerning their level of activity and heterotropic regulation. The relevance of these mutant structures to the kinetic data is discussed.

2. Materials and methods

2.1. Materials

Q-Sepharose Fast Flow resin was purchased from Pharmacia. Tris, malic acid, ampicillin, potassium dihydrogen phosphate, 2-mercaptoethanol, sodium EDTA, sodium azide and uracil were purchased from Sigma Chemical Co. Agarose, electrophoresis-grade acrylamide and enzyme-grade ammonium sulfate were purchased from ICN Biomedicals. Casamino acids, yeast extract and tryptone were obtained from Difco.

2.2. Strains

E. coli strain CJ236 [*dut*-1, *ung*-1, *thi*-1, *relA*-1/pCJ105(*Cm*$^{\rm r}$)] was obtained from T. Kunkel (NIEHS-Bethesda). M13K07 phage, pUC119 plasmid and *E. coli* K12 strain MV1190 [Δ(*lac-proAB*), *supE*, *thi*, Δ(*sri-recA*) 06::Tn10(*tet*)$^{\rm r}$/F′ *traD*36, *proAB*, *lacI*$^{\rm q}$, *lacZ*ΔM15] were obtained from J. Messing, Rutgers University.

2.3. Methods

2.3.1. Overexpression and purification of mutant enzyme. Asp19r→Ala and His20r→Ala enzymes were isolated from *E. coli* strain EK1104 (F$^-$ *ara*, *thi*, Δ*pro-lac*, Δ*pyrB*, *pyrF*$^{\pm}$, *rpsL*; Nowlan & Kantrowitz, 1985) containing either the pEK132 or pEK121 plasmid (Williams & Kantrowitz, 1998), which codes for the appropriate mutant enzyme. Enzymes were purified as described by Nowlan & Kantrowitz (1985).

2.3.2. Determination of protein concentration. The concentration of pure wild-type enzyme was determined from the absorbance at 280 nm using an extinction coefficient of 0.59 cm^2 mg^{-1} (Gerhart & Holoubek, 1967). The concentration of the mutant enzyme was determined using the Bio-Rad version of Bradford's dye-binding assay (Bradford, 1976) with the wild-type enzyme as a standard.

2.3.3. Crystallization of the mutant enzymes. Mutant enzymes were crystallized by the microdialysis method as described previously (Ke *et al.*, 1984) in the absence of effectors or substrate analogs. Hexagonal plate-shaped crystals appeared after approximately two weeks in a microdialysis chamber in which the enzyme concentration was 7.5 mg ml^{-1} and the buffer pH was 5.7. After an initial rapid-growth period, crystals grew slowly and reached a large size in a year. Crystals of His20Ar and Asp19Ar with approximate dimensions 1.2 × 1.2 × 0.2 and 0.6 × 0.4 × 0.1 mm, respectively, were mounted in glass capillaries prior to data collection.

2.3.4. X-ray data collection. Diffraction data were collected using a two-detector system on the San Diego multiwire area detector mounted on a Rigaku RU-200 rotating-anode generator operated at 50 kV and 150 mA at the Crystallographic Facility in the Chemistry Department of Boston College. The system is run by an ALPHA 3300 minicomputer. Diffraction data were collected to 2.15 Å from the His20Ar crystals and to 2.8 Å from the Asp19Ar crystals, with an $R_{\rm merge}$ of 0.071 and 0.101, respectively. Data sets were 94.2% and 91.2% complete for the respective mutants (His20Ar and Asp19Ar), with an average redundancy of 3.3 and 2.6.

X-ray data indicated space group *P*321 for both mutants. The unit-cell parameters were close to those of the wild-type T-state crystals as previously reported (Gouaux & Lipscomb, 1990; Honzatko *et al.*, 1982; Ke *et al.*, 1984). Data-collection and refinement statistics are summarized in Table 1.

2.3.5. Merging of reflections and structural refinement. Merging of reflections was performed using software provided by Area Detector Systems. The diffraction data were merged and edited until the $R_{\rm merge}$ converged (Table 1). The initial model for phasing and solution of the mutant structures consisted of the coordinates of the Thr82Ar mutant structure of *E. coli* aspartate transcarbamoylase (PDB code 1nbe), with respective residues replaced by alanine using the program *CHAIN*. Refinement was performed using *X-PLOR* v.3.1 (Brünger, 1992*b*) with cross-validation testing (Brünger, 1992*a*) and the Engh & Huber (1991) stereochemical parameters. Four working sets for the crystallographic R factor and test sets for the free R factor (10% of the reflections) were set up initially and followed during each stage of refinement. The refinement macrocycle usually consisted of simulated annealing in order to decouple working and free R factors (Brünger *et al.*, 1990) followed by positional refinement, temperature-factor refinement and automatic water-creation steps. Every step was checked against $R_{\rm free}$ and accepted or

rejected if the R_{free} increased or if the difference between R and R_{free} increased, respectively.

The models were further refined through cycles of simulated annealing using initial temperatures of up to 1000 K, positional refinement, temperature-factor refinement, automatic water addition and rigid-body refinement, bringing the free R factor down to ~0.24 and the final working R factor down to ~0.19 (Table 1). This extensive refinement resulted in improved electron-density maps.

At each stage of refinement, water molecules were automatically added using *IMPLOR* (Polyvision, Hopedale, Massachusetts, USA) at positions indicated by their density in OMIT maps ($F_o - F_c$). After each refinement cycle, the coordinates of water molecules with temperature factors greater than 69 Å^2 were deleted from the model and checked against the OMIT density after the next refinement cycle.

Refinements were carried out using Silicon Graphics Indigo II computers at Boston College. Refinement was considered complete when each of the available procedures, including water building, failed to further reduce the free R factor.

2.3.6. Structure comparisons. The procedure for structure comparison followed that developed for the Thr82Ar mutant enzyme as described previously (Williams *et al.*, 1998; Stieglitz *et al.*, 2004). The method is based on establishing the geometrical parameters that can be reliably compared between different structures. The program calculates the centers of gravity of individual domains from the C$^\alpha$-atom coordinates with loops excluded. We used the same set of atoms as established previously (Stieglitz *et al.*, 2004). The subsets consisted of (i) the C$^\alpha$ atoms of residues 15r–48r and 56r–100r, comprising the allosteric domain of the regulatory chain, (ii) the C$^\alpha$ atoms of residues 100r–128r and 134r–150r of the zinc domain of the regulatory chain and (iii) the C$^\alpha$ atoms of residues 1c–32c, 37c–74c, 87c–231c, 248c–269c and 273c–306c comprising the carbamoyl phosphate and aspartate domains of the catalytic chain[4]. The planar and torsional angles between the different domains were calculated based on the centers of gravity. Superposition of the wild-type and mutant structures and subsequent calculations of r.m.s. deviations were performed employing the molecular-similarity features of *QUANTA* (Accelrys).

2.3.7. Consensus modeling. The first element of the procedure was a traditional refinement in order to obtain the best possible model for fragments in the individual models of different mutants. This was achieved by obeying the stereochemistry and inspecting models at increasingly lower levels of the difference maps. This latter step served to establish a contouring level at which noise was not seen and was particularly important to establish a low level of the difference map that allowed us to see fragments that were not seen at higher contouring levels. We routinely reached a level of 0.6σ before observing noise. The excellent agreement of maps contoured at the customary 1.2σ and at 0.7σ levels was sufficient to proceed to the final stage of averaging maps for different mutants.

In the first step, maps of the same size were produced for the mutants using the same grid size at the same resolution for both mutants. Subsequently, maps were added and averages were calculated at every grid point. The map was then contoured and visualized in *CHAIN*. The resulting map was cleaner and provided more detail. However, the map had to be inspected at a slightly lower contouring level than the original maps to provide a similar level of detail.

3. Results

3.1. Quality of the structure of aspartate transcarbamoylase mutants

Crucial data-collection and refinement statistics are presented in Table 1. The quality of the structures was examined using the program *PROCHECK*. The side-chain and backbone geometrical parameters were within the expected values for the stereochemistry of a protein at this resolution. The Ramachandran plots of the φ–ψ angles of the final refined coordinates for the His20Ar and Asp19Ar mutant enzymes were very similar to the previously published Thr82Ar mutant and indicated that nearly all residues were in the most favored regions. The improved resolution in conjunction with other mutant structures allowed us to position the side chains in the most preferred conformations. Several structural changes were observed and are described below. The difference electron density calculated with the omission of regulatory-chain residues 19 and 20 clearly showed that both were occupied by alanine in the respective models (Fig. 2)

3.2. Modifications to protein structure

3.2.1. Common side-chain errors. Simultaneous determination of two mutant structures enabled us to analyze the model in great detail. The higher resolution of His20Ar (2.1 Å) allowed us to resolve uncertain elements in the lower resolution Asp19Ar structure, although occasionally the latter provided clearer answers to structural questions. Overall, 27% of the amino acids in the catalytic chain and 31% in the regulatory chain acquired a different conformation compared with previous determinations (PDB code 6at1). The most frequent changes were observed in Arg and Leu residues, which resulted in changes in polar and hydrophobic contacts, respectively. This type of correction is presented in Fig. 3. These corrections resulted in a low r.m.s.d. for angles in the final model for both mutants (see Table 1 and Fig. 3).

3.2.2. Possible disorder. Based on previous reports of disordered residues (Stevens *et al.*, 1990), we inspected the model for possible disorder. Of the disordered residues reported previously, most were identified in a single conformation, with the exception of Arg54. An example of the electron density for Arg54 is presented in Fig. 4. Temperature factors are usually the best indicators of possible disorder or conformational variability. The average temperature factors

[4] The two domains of the catalytic chain are identified by the substrates they bind: namely, the aspartate domain (ASP) and the carbamyl phosphate domain (CP). The two domains of the regulatory subunit are named the zinc domain (ZN) and the allosteric domain (ALL).

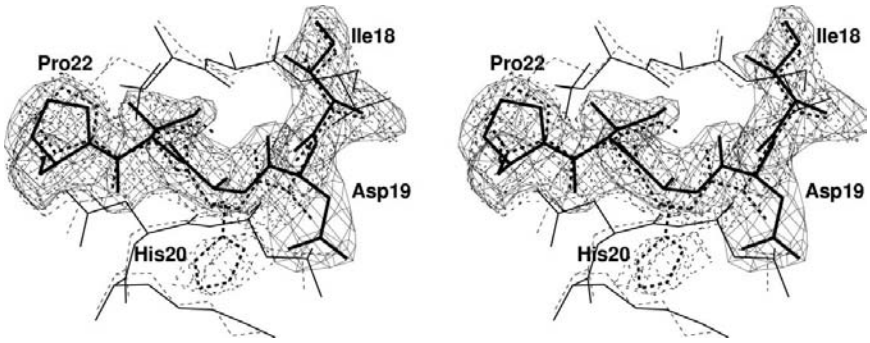

Figure 2
Superposition of the three strands of the r1 regulatory-chain structure of the two mutants (His20Ar, continuous lines; Asp19, broken lines) covered by the electron density of the two mutants (His20, continuous lines; Asp19Ar, broken lines) contoured at the 1.2σ level. The figure shows a lack of density at the mutated residue site.

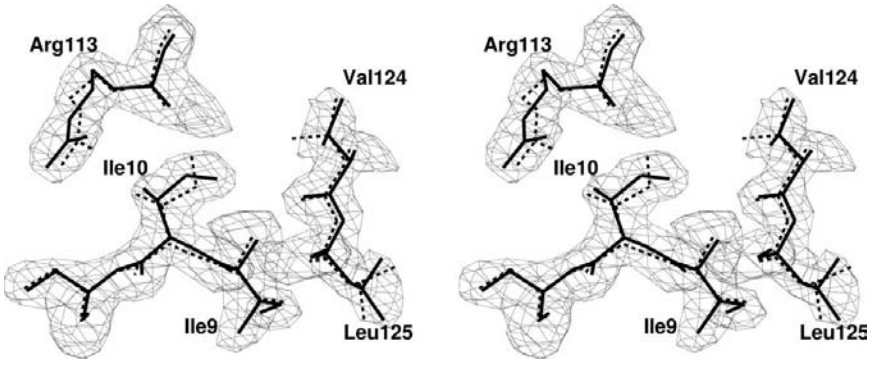

Figure 3
Superposition of the wild-type model of the T-state (broken lines; PDB code 1rah) with the His20Ar model at the well refined region of the catalytic subunit, showing the most common changes at Arg, Leu, Ile and Val head groups. The $2F_o - F_c$ electron density was calculated using the His20Ar full-atom model contoured at the 1.5σ level.

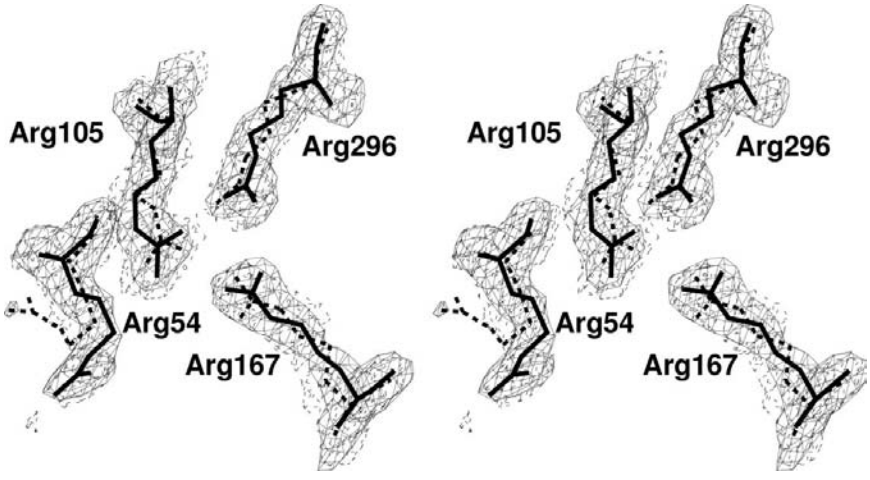

Figure 4
Arginine residues near the active site are visualized covered by $2F_o - F_c$ electron-density maps calculated from atomic models of the His20Ar (continuous lines) and Asp19Ar (broken lines) mutants. The His20Ar model is in thick lines and thick broken lines indicate the wild-type 1rah model.

for the described models are presented in Table 1. The only fragments with increased mobility were the 80s and 240s loops and the C-terminal fragment of the catalytic subunit and the N-terminal fragment and the 50s and 130s loops of the regulatory subunit.

3.2.3. 240s loops. Several portions of the backbone had elevated temperature factors in earlier models, including portions of the 240s loop. To investigate these fragments in more detail, we inspected the OMIT maps at the 240s loop. Alternative densities were observed and the model was rebuilt. Instead of an extended loop analogous to the R-state structure, the backbone formed one additional turn in a continuation of the existing α-helix. This fragment refined well as a 3_{10}-helix terminating the 237–243 α-helix present in both the T- and the R-state models. This change of local backbone conformation was confirmed in all of our models of mutant enzymes (Fig. 5). A comparison with the R-state structure (PDB code 1d09; Jin *et al.*, 1999) shows a conformational change is necessary to carry the enzyme from the T-state to the R-state. This change requires a flip of two peptide bonds at residues 44–45 and 45–46. In this new model Lys244 participates in hydrogen bonds to Asp271, which is also hydrogen-bonded to Tyr240 (Figs. 5*a* and 5*b*). The importance of this interaction for the allosteric transition has been evaluated and described previously (Alam *et al.*, 2004).

3.2.4. The 80s loop attains two conformations despite consensus modeling. Historically, the 80s loop in T-state models has shown weak density and suggested possible disorder. Localizing it presented a significant difficulty. At first glance the loop appears to be too long to span two structural elements, such as strand S3 and helix H3 of the carbamyl phosphate domain of the catalytic subunit. Its full functional role is revealed only in the R-state, in which Ser80 and Lys84 participate in formation of the active site of the neighboring subunit and the loop is then well ordered with low temperature factors. These observations suggest that the loop is important for catalytic activity and communication between subunits.

When applied to the loop, the consensus modeling method described in §2 indicated that there were two prevalent conformations for the loop. One is semi-folded in a manner similar to that refined before

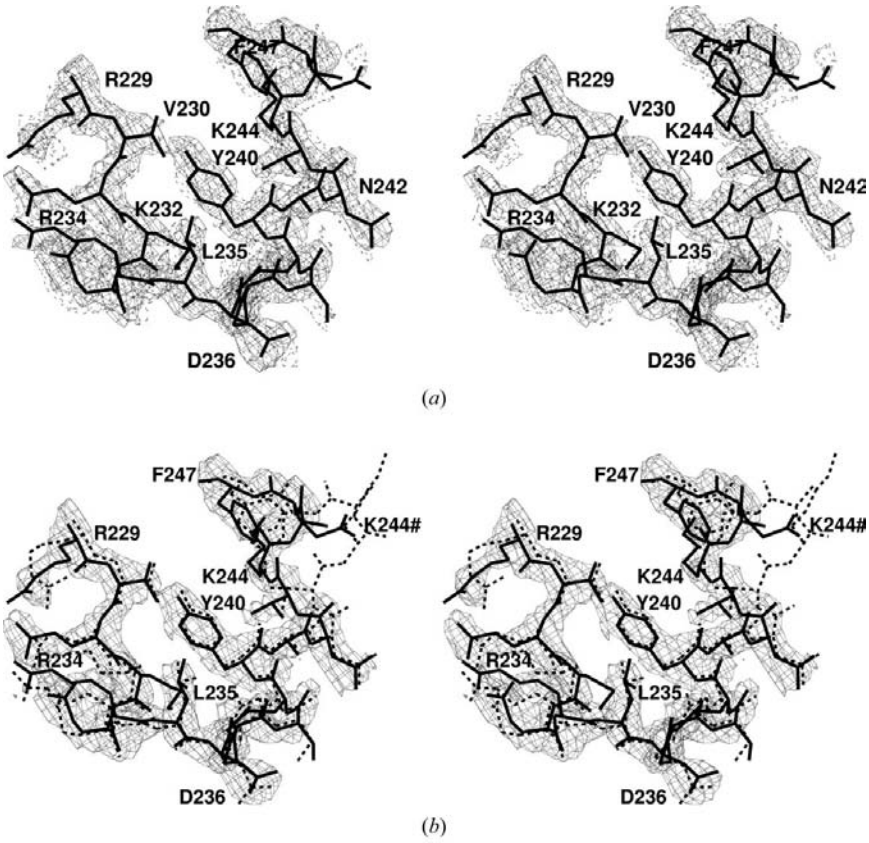

Figure 5
(*a*) The residues of the 240s loop are shown covered by $2F_o - F_c$ electron-density maps (contoured at 1.2σ) calculated from the His20Ar atomic model. The atomic model for His20Ar is presented in thick lines, while the wild-type 1rah model (Kosman *et al.*, 1993) is depicted in broken lines. (*b*) The same fragment of the His20Ar model covered by a consensus-averaged map. Note the high quality of the averaged map.

(Stevens *et al.*, 1990; Kosman *et al.*, 1993), while the other is more extended. An extended-conformation model better fits the data for the His20Ar mutant, while the Asp19Ar molecular model is more traditionally folded. For comparison, in Fig. 6 we present electron densities of appropriate models for His20Ar and Asp19Ar superimposed with consensus maps produced by averaging maps for both mutants.

3.2.5. 50s and 130s loops. The mobile elements, the 50s and 130s regions of the regulatory domain of the final models, produced averaged maps that were cleaner than the maps originally obtained for both mutant enzymes. The consensus modeling procedure allowed us to establish with high accuracy the most likely positioning of those fragments. The resulting models are presented in Figs. 7(*a*), 7(*b*) and 7(*c*), in which we compare the 50s loops and 130s loops of the regulatory chains to the conformations of the wild-type enzyme, as reported by Kosman *et al.* (1993) (PDB code 1rah).

3.2.6. The N-terminus. In the majority of the previously determined structures of ATCase the N-terminal fragments of the regulatory domains were not refined. Apparently, the quality of the electron density was low and represented a formidable challenge to the derivation of a reliable model. The model of Kosman *et al.* (1993) constituted the starting point for the search.

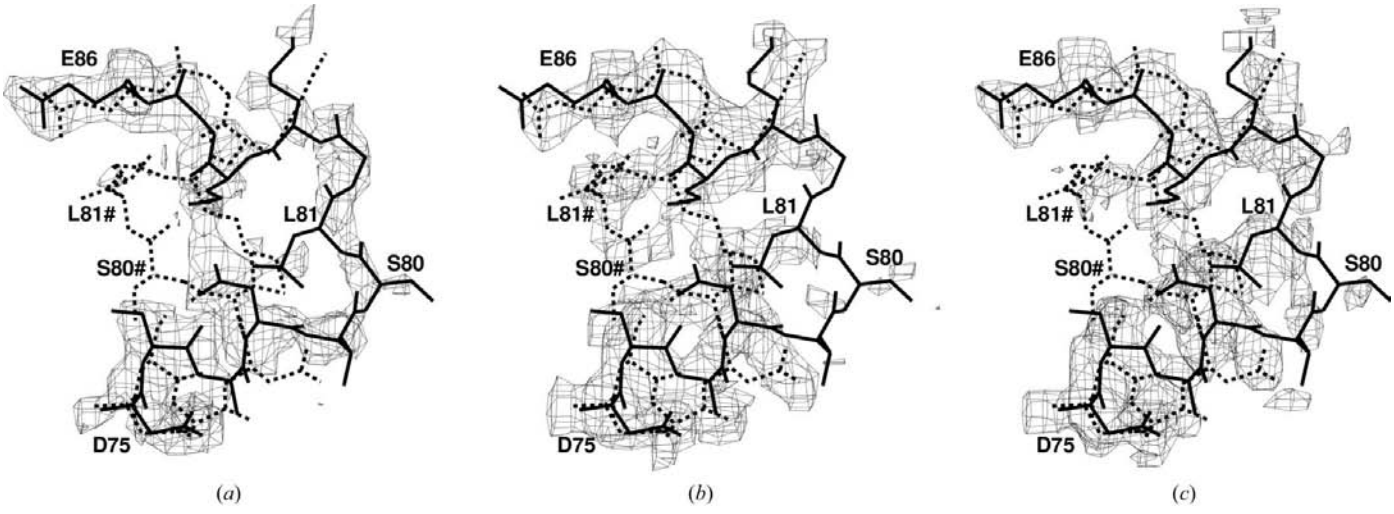

Figure 6
Different models of the 80s loop: His20Ar model in thick lines, Asp19Ar model in broken lines. (*a*) The His20Ar model covered by the electron density calculated from the mutant atomic model. (*b*) The Asp19Ar model covered by the electron density calculated from the atomic coordinates of the mutant. (*c*) The consensus map shows two solutions for the conformation of the 80s loop. All maps are contoured at the 1σ level.

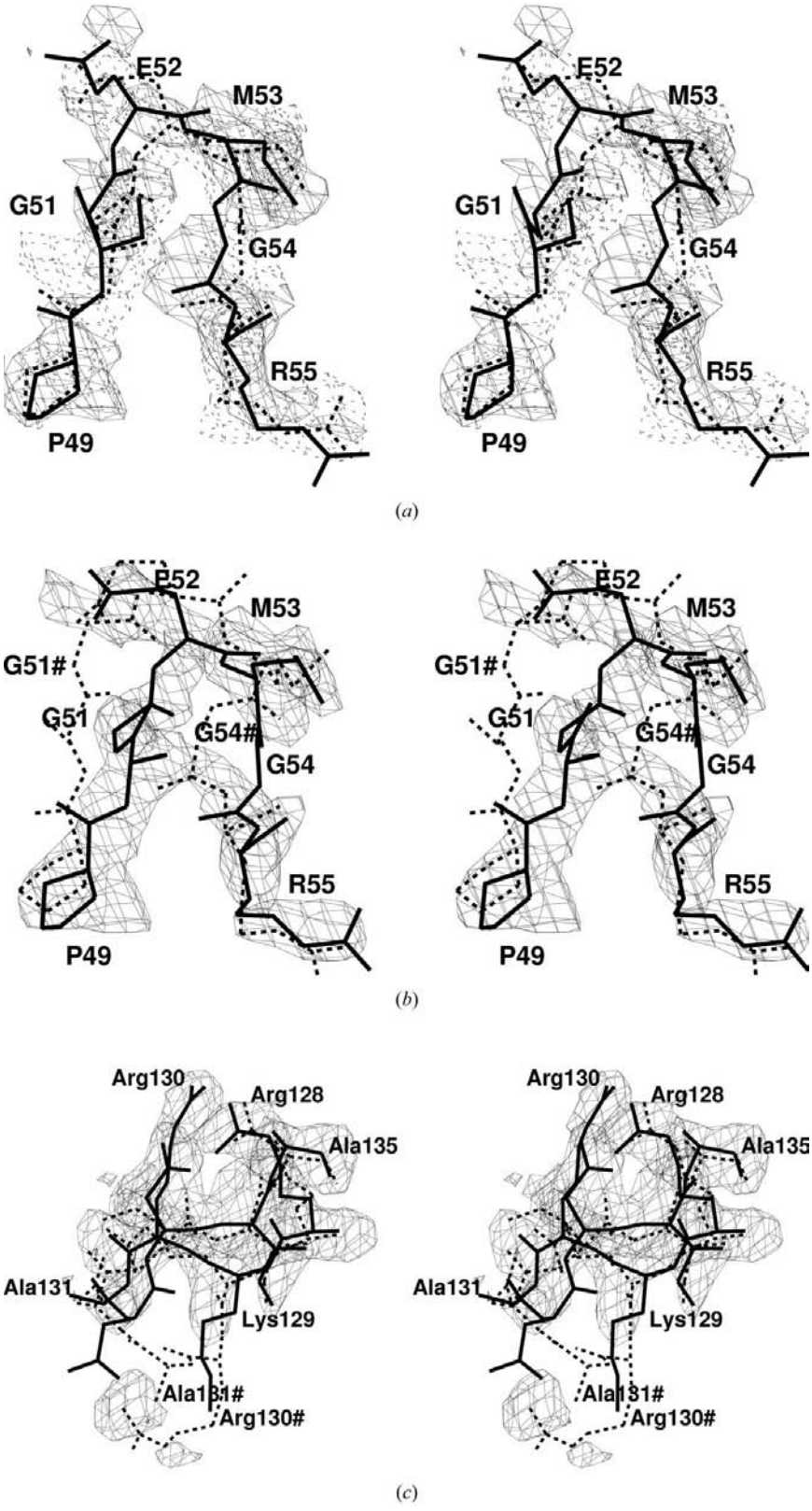

Figure 7
(*a*) Model of the 50s loop with His20Ar (continuous lines) and Asp19Ar (broken lines) superposed on the electron densities of both mutants. (*b*) The 50s loop with the Asp19Ar model superposed on the wild-type 1rah model covered by the consensus-averaged map. (*c*) Model of the 130s loop visualized with the His20 model in continuous lines and the 1rah model in broken lines covered by the consensus electron-density map (contour level 1σ).

Our detailed refinement did not confirm this model. We extensively used difference electron-density maps to establish the most probable conformation of these fragments. At the end of the process, we obtained stable refined structures for the initial ten residues in both mutant structures, but the electron-density maps were not of high quality and the temperature factors indicated high mobility.

To objectify the modeling process, we attempted to use the consensus modeling technique. However, in this case it did not help to provide better descriptions of the fragments derived from the difference Fourier methods. An element that is common to all refined models of the wild type as well as the mutant enzymes was the disappearance of the electron-density map at position 9. Weak but interpretable electron density was observed upstream of position 9, allowing the tracing of the initial seven residues in each subunit. In both subunits the polypeptide backbone protruded into the corresponding nucleotide effector-binding site. The models for the r1 and r6 N-termini differed from each other, creating some asymmetry, as seen in Figs. 8(*a*) and 8(*b*).

3.2.7. Modifications to interface domain contacts. Interface domain contacts, defined as contacts closer than 3.5 Å capable of making an electron-donor/acceptor pair, were determined for both mutants and compared with those of the wild-type 6at1 structure (Stevens *et al.*, 1990). The carbamoyl phosphate and the aspartate domain interface, the carbamoyl phosphate and the zinc domain interface, the c1–c2 interface and the r1–r6 interface were largely unchanged. However, significant changes in contacts occurred between the allosteric and zinc domain interface, the aspartate and zinc domain interface (c1–r1) and the c1–c4 interface (Table 2). Furthermore, several changes in hydrogen-bond contacts in the catalytic trimer interfaces were observed in the His20Ar structure compared with the wild-type structure and to a lesser degree the Asp19Ar structure.

3.3. Geometrical and conformational analysis

In order to understand the origin of the large r.m.s. deviation observed on the superposition of the entire regulatory chain,

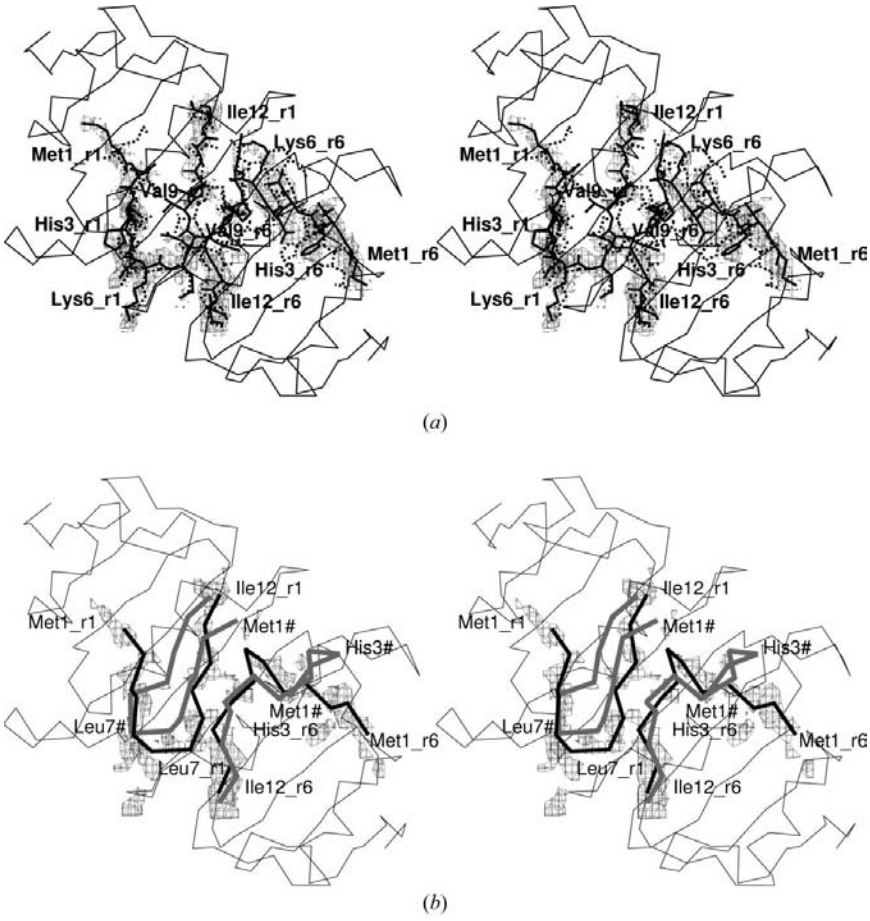

Figure 8
Model of the N-terminal region of the regulatory subunit of the mutant enzymes. (*a*) Both models are shown covered by electron-density maps (continuous lines, His20Ar; broken lines, Asp19Ar). The maps are contoured at 0.8σ. (*b*) The consensus map is shown. The map is of lesser quality than the individual mutant maps. Models shown are the His20Ar model (heavy line) and the N-termini model proposed by Kosman *et al.* (1993) (gray line).

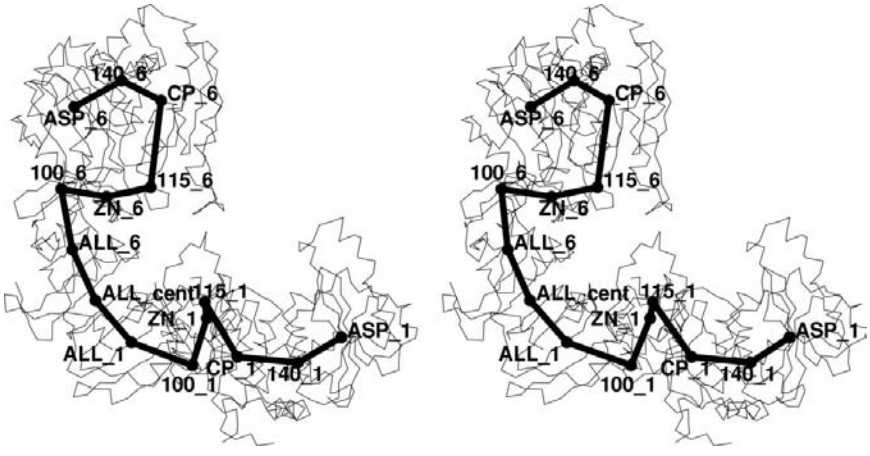

Figure 9
A stereo representation of an asymmetric unit of the ATCase structure (two catalytic and two regulatory subunits) with the heavy line connecting the geometrical centers of the domains and the hinges (see §2) which served to define the angles between the domains.

we used a previously described protocol (Stieglitz *et al.*, 2004). The ZN domains of the regulatory chains were used as the reference domain for superposition of the wild-type and mutant structures. The relative position and r.m.s. deviation of the ALL domain and catalytic chains were then reported in reference to the ZN-domain superposition (Fig. 9 and Table 3). The large deviation of the ALL domain on r1 and r6 superposition suggests a tertiary and quaternary structural change of the mutant ALL domain relative to the conformation and location of the wild-type ALL domain (Table 3).

Our previous experience indicated that selecting ZN domains for superposition and calculating the deviation of the catalytic chain optimized the detection of relevant structural changes. The r.m.s. deviation was 0.23 Å when the ZN domain of the wild-type r1 chain and the ZN domain of the His20Ar r1 regulatory chain were superimposed. The same domains superimposed with Asp19Ar gave an r.m.s. deviation of 0.35 Å. For ASP and CP domains, the r.m.s. deviations were 0.23 and 0.34 Å for His20Ar and Asp19Ar, respectively.

4. Discussion

4.1. Evaluation of consensus modeling

The quality of the electron-density map was sufficiently high to allow revision of the conformation of not only the side-chain groups of several amino acids but also of five fragments of the protein backbone compared with earlier models (PDB code 6at1). Two revisions to the backbone were in the catalytic chain, including the 240s and 80s loops. At the level of a single model, the change in the conformation of the 240s loop resulted in a well defined 3_{10}-helix at the end of an α-helix (Fig. 5), while the modifications introduced in the 80s loop improved the model, although weak electron density persisted. A similar situation exists in the regulatory chain, where despite improvements the traditionally weak density for the 50s and 130s loops and the N-terminal fragment persisted.

The consensus modeling technique allowed us to reliably model fragments that were not clearly resolved in previous structures and to unequivocally establish conformations for the 240s loop in the catalytic

Table 2
Comparison of the interactions at subunit interfaces for the His20Ar and Asp19Ar mutants, and the Thr82Ar mutant and wild-type unliganded T-states.

Calculations are based on structures generated with `surface_plot.inp` and `buried_plot.inp` in *CNS*. The program *DIMPLOT* was used to identify specific hydrogen-bonding donors and acceptors at interfaces at a cutoff of 3.75 Å for hydrogen bonding and 4.8 Å for salt-bridge (ionic) interactions.

	Structure			
Interface	His20Ar	Asp19Ar	Thr82Ar†	Wild-type ATCase‡
By domain				
r1 AL–ZN	6	10	15	11
r6 AL–ZN	4	8	13	9
By chain				
c1–c4	12	14	8	4
r1–c4	4	10	7	6
c1–r1	9	14	20	16
r1–r6	10	13	18	14
c6–r6	7	14	16	14

† PDB code 1nbe. ‡ PDB code 6at1.

Table 3
R.m.s.d.s (Å) for the pairwise superimposition of different domains of ATCase mutants with the wild type.

	Domain							
Protein	CP1	ASP1	ZN1	ALL1	ALL6	ZN6	ASP6	CP6
6at1/His20Ar	0.224	0.295	0.233	0.395	0.552	0.231	0.233	0.208
6at1/Asp19Ar	0.346	0.433	0.348	0.507	0.613	0.348	0.435	0.347

Table 4
Angles between mobile units in different forms and mutants of ATCase.

	Angle (°)						
Protein	CP1–ASP1	CP6–ASP6	CP1–ZN1	CP6–ZN6	ZN1–ALL1	ZN6–ALL6	ALL1–ALL6
1d09, R-state	127.71	128.35	111.15	110.80	104.36	103.18	155.84
8at1, R-state	127.64	127.41	110.71	110.54	105.55	102.63	155.52
6at1, T-state	134.11	135.69	111.17	111.26	105.56	105.62	153.28
His20Ar	135.93	136.67	113.55	110.38	105.94	103.24	155.05
Asp19Ar	134.17	136.78	112.61	110.42	101.92	103.71	155.28

Table 5
Torsional angles (°) around the twofold and threefold axes of ATCase mutants.

	Protein				
Angle	1d09, R-state	8at1, R-state	6at1, T-state	His20Ar, T-state	Asp19Ar, T-state
Twofold	25.33	21.98	40.01	39.81	39.48
Threefold	−77.32	−77.10	−88.30	−88.11	−88.16

chain and the 50s and 130s loops in the regulatory chain. The technique resulted in two distinct conformations when applied to the 80s loop of the catalytic subunit. The only regions where the technique did not provide substantial new information beyond the original electron-density maps were the N-termini of the regulatory subunits. Despite weak density in the N-terminal region of the regulatory chain, we constructed a tentative model for the first ten residues in both of the regulatory chains that differs from a previous report (Kosman *et al.*, 1993). In addition, we observed numerous small conformational changes in the nucleotide-binding pocket associated with the deletion of the Asp19 or His20 side chain.

4.2. Local changes in the nucleotide-binding pocket

The crystal structures of the wild-type enzyme have revealed several contacts between the backbone and side chains of residues Asp19r, His20r, Lys94r and Thr82r, and the ATP and CTP phosphate moieties (Gouaux & Lipscomb, 1990; Gouaux *et al.*, 1990; Kosman *et al.*, 1993; Stevens *et al.*, 1990). Those interactions are likely to be responsible for properly orienting the nucleotide in the binding site and are therefore likely to be crucial for the affinity of the enzyme for nucleotides and/or for maximal activation and inhibition.

Substitutions at positions 19 and 20 may not directly influence the global conformation of the binding pocket. However, comparison with the wild-type CTP-ligated and unligated structures shows that there is a conformational change (Table 3). His20 swings in and out of the pocket depending on the presence of the nucleotide effector. In the CTP-ligated structure (PDB code 1rah; Kosman *et al.*, 1993), His20 forms a hydrogen bond to the CTP γ-phosphate. In addition, His20 forms a hydrogen bond to Asp19, which further forms a hydrogen bond to Lys56 (Fig. 1). These interactions may stabilize the protonated form of His20. The conformational change detected in His20 might reflect the natural change upon nucleotide binding (a molecular switch) coupled to the change in conformation of Lys56. Substitution of either His20 or Asp19 by alanine destabilizes the His20–Asp19–Lys56 network, which results in changes in heterotropic response as it may hinder nucleotide binding. A similar effect was seen previously in the mutation of Lys56 to alanine (Stevens *et al.*, 1991).

The mutants described here may also indirectly influence the binding pocket by influencing the polar/ionic network *via* interaction of the Glu62r and Lys6r residues with the N-terminus. This is implied based on previous work that suggested that the N-terminus plays the role of a 'lid' closing nucleotides into the binding pocket of the allosteric domain. More recent studies show that His3r, Asp4r and Lys6 coordinate CTP or UTP in the structures of these complexes (KSJ, unpublished results).

4.3. Alterations at subunit interfaces suggest a compensatory mechanism for His20Ar and Asp19Ar mutants to remain in the T-state

Crystal studies of wild-type aspartate transcarbamoylase reveal structural asymmetry between the r1 and r6 regulatory chains (Ke *et al.*, 1988; Kim *et al.*, 1987; Stevens *et al.*, 1990) which may be directly associated with the allosteric state of the enzyme (Stieglitz *et al.*, 2004). A closer inspection of the ψ

conformational angle between the ZN and allosteric domains reveals a dependence of this angle on the stabilization form of the mutant (Table 4). There is a degree of correlation between the change of the planar angle between the domains in the catalytic subunit and T- or R-state stabilization. Surprisingly, the angle between the Zn and CP domains also changes what is otherwise considered to be a stable interface. These two angles are the most sensitive probes for stabilization.

Changes in this planar angle also correlate with the altered polar contacts seen in the AL–ZN interfaces for both r1 and r6. In the case of His20Ar there is a slight decrease in polar interactions at this interface, whereas in Asp19Ar there is an increase relative to the super-twisted T-state Thr82Ar and the unliganded wild-type form (PDB code 6at1; Kosman *et al.*, 1993). Those trends continue in the r1–c4, c1–r1, c6–r6 and r1–r6 interfaces, implying that at these interfaces T-state stabilizing interactions are tightened for unliganded Asp19Ar and loosened for unliganded His20Ar. In the case of Asp19Ar, this may be interpreted as an 'overtightening of a screw' mechanism to hold these structures in the T-state in the absence of effectors and substrates. Further studies with ligands are required to test the predictions derived from these two structures. Altered subunit contacts at the interfaces are primarily responsible for loss of symmetry and may represent compensatory interactions to minimize divergence from the equilibrium state.

The interdomain contacts between the r1 and c4 subunits show an effect that is opposite to the other interactions (Table 2). Previous studies with site-specific mutants indicated that many of these interfaces stabilize the T-state of aspartate transcarbamoylase (Kantrowitz & Lipscomb, 1990). In fact, the r1–c4 and c1–c4 and symmetry-related interface contacts are broken upon the quaternary transition from the T-state to the R-state (Ke *et al.*, 1988; Lipscomb, 1994). The observed structural alterations in these contacts may stabilize the T–R equilibrium in favor of the T-state and explain the observed T-state stabilization of previously described mutants; *e.g.* for Thr82Ar kinetic analysis showed T-state stabilization, while the structure was termed an extreme T-state (Williams & Kantrowitz, 1998).

4.4. Relevance of His20Ar and Asp19Ar mutant structures to kinetic studies of heterotropic effects

Analysis of torsional angles around the twofold and threefold axes show rotation of the mutant regulatory dimer approximately 1° further towards the R-state (in His20Ar) and toward the T-state (in Asp19Ar) relative to the wild-type enzyme (Tables 4 and 5). However, structural analysis of the upper compared with the lower catalytic trimer indicated no significant rotation along the molecular threefold axes of symmetry compared with the wild-type enzyme. These small changes observed in the absence of global expansion along the threefold axis may indicate initial steps away from T-state equilibrium, as reported by Stieglitz *et al.* (2004).

Alterations in polar interactions (Table 2) in either the Asp19Ar or His20Ar mutant compared with the wild-type enzyme clearly show that perturbation of this interaction has far-reaching effects on subunit interfaces. This effect is a consequence of the fact that His20 and Asp19 are part of an extensive polar/ionic network of discrete side-chain and backbone interactions spanning the allosteric β-sheet domain. This network directly influences the nucleotide-binding site *via* the Lys6r and Glu62r salt-bridge interaction, suggesting overall that His20 and Asp19 synergize as 'molecular modulators' to control enzyme equilibrium in the presence of heterotropic effectors.

This work was supported by Grant GM26237 to ERK from the National Institute of General Medical Sciences.

References

Alam, N., Stieglitz, K. A., Caban, M. D., Gourinath, S., Tsuruta, H. & Kantrowitz, E. R. (2004). *J. Biol. Chem.* **279**, 23302–23310.

Bradford, M. M. (1976). *Anal. Biochem.* **72**, 248–254.

Brünger, A. T. (1992*a*). *Nature (London)*, **355**, 472–475.

Brünger, A. T. (1992*b*). *X-PLOR* v.3.1. *A System for Crystallography and NMR*. Yale University Press, New Haven, Connecticut, USA.

Brünger, A. T., Krukowski, A. & Erickson, J. W. (1990). *Acta Cryst.* A**46**, 585–593.

Dembowski, N. J. & Kantrowitz, E. R. (1994). *Protein Eng.* **6**, 673–679.

Engh, R. A. & Huber, R. (1991). *Acta Cryst.* A**47**, 392–400.

England, P. & Hervé, G. (1994). *Biochemistry*, **33**, 3913–3918.

Gerhart, J. C. & Holoubek, H. (1967). *J. Biol. Chem.* **242**, 2886–2892.

Gerhart, J. C. & Pardee, A. B. (1962). *J. Biol. Chem.* **237**, 891–896.

Gerhart, J. C. & Schachman, H. K. (1968). *Biochemistry*, **7**, 538–552.

Gouaux, J. E. & Lipscomb, W. N. (1990). *Biochemistry*, **29**, 389–402.

Gouaux, J. E., Stevens, R. C. & Lipscomb, W. N. (1990). *Biochemistry*, **29**, 7702–7715.

Hervé, G., Moody, M. F., Tauc, P., Vachette, P. & Jones, P. T. (1985). *J. Mol. Biol.* **185**, 189–199.

Honzatko, R. B., Crawford, J. L., Monaco, H. L., Ladner, J. E., Edwards, B. F. P., Evans, D. R., Warren, S. G., Wiley, D. C., Ladner, R. C. & Lipscomb, W. N. (1982). *J. Mol. Biol.* **160**, 219–263.

Howlett, G. J. & Schachman, H. K. (1977). *Biochemistry*, **16**, 5077–5083.

Jin, L., Stec, B., Lipscomb, W. N. & Kantrowitz, E. R. (1999). *Proteins*, **37**, 729–742.

Jones, M. E., Spector, L. & Lipmann, F. (1955). *J. Am. Chem. Soc.* **77**, 819–820.

Kantrowitz, E. R. & Lipscomb, W. N. (1990). *Trends Biochem. Sci.* **15**, 53–59.

Ke, H.-M., Honzatko, R. B. & Lipscomb, W. N. (1984). *Proc. Natl Acad. Sci. USA*, **81**, 4027–4040.

Ke, H.-M., Lipscomb, W. N., Cho, Y. & Honzatko, R. B. (1988). *J. Mol. Biol.* **204**, 725–747.

Kim, K. H., Pan, Z., Honzatko, R. B., Ke, H.-M. & Lipscomb, W. N. (1987). *J. Mol. Biol.* **196**, 853–875.

Kosman, R. P., Gouaux, J. E. & Lipscomb, W. N. (1993). *Proteins*, **15**, 147–176.

Lipscomb, W. N. (1994). *Adv. Enzymol.* **68**, 67–151.

Moody, M. F., Vachette, P. & Foote, A. M. (1979). *J. Mol. Biol.* **133**, 517–532.

Nowlan, S. F. & Kantrowitz, E. R. (1985). *J. Biol. Chem.* **260**, 14712–14716.

Reichard, P. & Hanshoff, G. (1956). *Acta Chem. Scand.* **10**, 548–560.

Sakash, J. B. & Kantrowitz, E. R. (1998). *Biochemistry*, **37**, 281–288.

Sakash, J. B., Tsen, A. & Kantrowitz, E. R. (2000). *Protein Sci.* **9**, 53–63.

Stevens, R. C., Chook, Y. M., Cho, C. Y., Lipscomb, W. N. & Kantrowitz, E. R. (1991). *Protein Eng.* **4**, 391–408.
Stevens, R. C., Gouaux, J. E. & Lipscomb, W. N. (1990). *Biochemistry*, **29**, 7691–7701.
Stieglitz, K., Stec, B., Baker, D. B. & Kantrowitz, E. R. (2004). *J. Mol. Biol.* **341**, 853–68.
Williams, M. K. & Kantrowitz, E. R. (1998). *Biochem. Biophys. Acta*, **1429**, 249–258.
Williams, M. K., Stec, B. & Kantrowitz, E. R. (1998). *J. Mol. Biol.* **281**, 121–134.
Yates, R. A. & Pardee, A. B. (1956). *J. Biol. Chem.* **221**, 757–770.